Theoretical analysis of numerical aperture increasing lens microscopy

S. B. Ippolito, B. B. Goldberg, and M. S. Ünlü
Departments of Physics and Electrical and Computer Engineering and the Photonics Center, Boston University, 8 Saint Mary's Street, Boston, Massachusetts 02215

(Received 3 August 2004; accepted 14 December 2004; published online 11 February 2005)

We present a detailed theoretical analysis and experimental results on a subsurface microscopy technique that significantly improves the light-gathering, resolving, and magnifying power of a conventional optical microscope. The numerical aperture increasing lens (NAIL) is a plano-convex lens placed on the planar surface of an object to enhance the amount of light coupled from subsurface structures within the object. In particular, a NAIL allows for the collection of otherwise inaccessible light at angles beyond the critical angle of the planar surface of the object. Therefore, the limit on numerical aperture increases from unity for conventional subsurface microscopy to the refractive index of the object for NAIL microscopy. Spherical aberration associated with conventional subsurface microscopy is also eliminated by the NAIL. Consequently, both the amount of light collected and diffraction-limited spatial resolution are improved beyond the limits of conventional subsurface microscopy. A theoretical optical model for imaging structures below the planar surface of an object, both with and without a NAIL, is presented. Experimental results demonstrating the predicted improvements in resolution of subsurface imaging are also presented. © *2005 American Institute of Physics*. [DOI: 10.1063/1.1858060]

I. INTRODUCTION

Many subsurface optical microscopy applications, such as Si integrated circuit (IC) failure analysis, spectroscopy of single quantum dots, and optical data storage, require operation near the ultimate limits of light-gathering and resolving power, beyond the capability of conventional subsurface microscopy. In the absence of aberrations, the diffraction of light limits the spatial resolution of a conventional optical microscope to $\approx\lambda_0/2n \sin\theta_a$ laterally and $\approx\lambda_0/n(1-\cos\theta_a)$ longitudinally, where λ_0 is the free space wavelength of light, n is the refractive index of the object space, and θ_a is the angular semiaperture in the object space.[1] The numerical aperture (NA), $n \sin\theta_a$, is the most common measure of light-gathering power, because of its inverse relationship with the diffraction limit of lateral spatial resolution. Increasing θ_a improves the spatial resolution and increases the amount of light collected. Reducing the wavelength of light by either decreasing λ_0 or increasing n also improves the spatial resolution. Conventional optical microscopy may be divided into two modes, according to the location of the focus in the object space: surface optical microscopy and subsurface optical microscopy. In Sec. I A, surface optical microscopy techniques and a brief review of experimental results are presented, providing a background for the terminology established for the numerical aperture increasing lens (NAIL) subsurface optical microscopy technique presented in Sec. I B. In Sec. II, a theoretical optical model for imaging subsurface structures in an object with a planar surface, first without, then with a NAIL, is presented in Secs. II A and II B, respectively. In Sec. II C, the theoretical results are compared, and finally, in Sec. III, agreement between the theoretical and experimental results is confirmed.

A. Surface optical microscopy

Conventional optical microscopy of the surface of an object is illustrated schematically in Fig. 1(a). The refractive index of air in the object space is unity, which limits the NA to unity and ultimately limits the lateral spatial resolution to $\approx\lambda_0/2$ and the longitudinal spatial resolution to $\approx\lambda_0$. Many surface optical microscopy techniques have been developed to improve spatial resolution beyond the limits of conventional optical microscopy, by placing additional elements in the optical near-field of the surface of an object.

Immersion techniques introduce a medium with a high refractive index n into the object space, above the surface of an object. This increases the limit on the NA to n, and improves the ultimate limit on the lateral spatial resolution to $\approx\lambda_0/2n$ and the longitudinal spatial resolution to $\approx\lambda_0/n$. In liquid immersion microscopy, the region between a liquid immersion objective lens and the surface of an object is filled with an immersion liquid, such as water or oil with a refractive index up to 1.6, as illustrated in Fig. 1(b). Hence, the

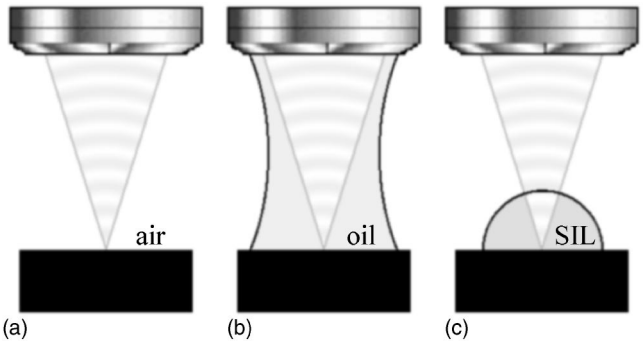

FIG. 1. Imaging the surface of an object with (a) a conventional optical microscope, (b) an oil immersion microscope, and (c) a solid immersion lens microscope.

optical near-field of the object is immersed in liquid. Despite the significant improvements in the NA and spatial resolution, the drawbacks of liquid immersion microscopy include the contamination of an object and a small working distance.

The solid immersion lens (SIL) technique places a plano-convex lens on the surface of an object, as shown in Fig. 1(c).[2] In this case, the optical near-field of the object is immersed in a solid. The SIL can have a refractive index up to 4, depending on the free space wavelength of light and the material selected. To date, Si, GaP, GaAs, sapphire, and glass SILs have been successfully fabricated and experimentally demonstrated. The SIL technique was first proposed and demonstrated by Mansfield and Kino to clearly resolve 100 nm lines and spaces in photoresist, with light at a λ_0 of 436 nm, using a glass SIL.[2] Since then, the SIL technique has been applied to a variety of applications to improve spatial resolution. In optical data storage, the SIL technique increased information density by a factor of 4.[3–5] Low temperature photoluminescence microscopy studies of low dimensional semiconductor structures, using a SIL, have revealed important physical phenomena and material properties.[6–14] The SIL technique has been used in ultrafast pump-probe spectroscopy of a quantum well structure to study lateral carrier transport.[15] In fluorescence microscopy, the SIL has not only yielded increased spatial resolution but also increased the amount of light collected.[16–18] The SIL technique has also been used in micro-Raman spectroscopy of patterned Si,[19] and has been suggested as a way of increasing the resolution of photolithography,[20] as well as being used to measure the laser power of highly divergent beams.[21] For most of the aforementioned experiments, the diameter of the SIL was a few millimeters. However, a microfabricated SIL with a diameter of 15 μm has also been demonstrated.[22–24] Despite the significant improvements in NA and spatial resolution, the major drawback of SIL microscopy is that direct physical contact with an object is necessary. In summary, both solid and liquid immersion techniques have been shown to improve spatial resolution by introducing a medium with a high refractive index into the object space.

B. Subsurface optical microscopy

If an object consists of structures buried within a transparent and homogeneous medium with an optical quality surface, then its subsurface structures may be imaged with an optical microscope. The encapsulating medium, through which light must propagate, provides additional optical constraints—the range of λ_0 where it is transparent, its refractive index n, as well as the reflection and refraction at its surface. Once the lowest possible value of λ_0/n for the encapsulating medium is selected, the spatial resolution can only be improved by altering the surface geometry of the encapsulating medium. Ideally, the surface geometry should maximize the angular semiaperture in the object space θ_a, and introduce no significant aberrations, to permit operation at the diffraction limit.

A planar surface geometry is the most common type of surface geometry, as it is either characteristic of an object or producible by polishing or cleaving. Figure 2(a) illustrates a conventional optical microscope imaging subsurface structures in an object with a planar surface. Reflection and refraction at the planar surface of an object limits a conventional optical microscope's light-gathering power from subsurface structures within the object. Reflection at the planar surface of an object reduces the amount of light that escapes from the object, allowing no light to escape above the critical angle θ_c, which is, by definition, $\sin^{-1}(1/n)$. According to Snell's law, refraction at the planar surface of an object reduces $\sin\theta_a$ for a given objective lens by a factor of n; however, the NA remains the same because of the increased refractive index in the object space. Refraction also imparts spherical aberration that increases monotonically with angle, thereby requiring correction to operate at the diffraction limit. The absence of light from above the critical angle ultimately limits the lateral spatial resolution to $\approx\lambda_0/2$ and the longitudinal spatial resolution to $\approx\lambda_0 n(1+\cos\theta_c)$. Thus, despite the advantage of having a higher refractive index of the encapsulating medium in relation to the refractive index of air, the subsurface spatial resolution is always worse than the surface spatial resolution in conventional optical microscopy of an object with planar surface geometry. Circumventing this planar surface barrier would yield significant improvement in the amount of light collected and the spatial resolution. Despite these limitations, because of convenience, a conventional optical microscope is commonly used for subsurface imaging of objects with planar surface geometry.

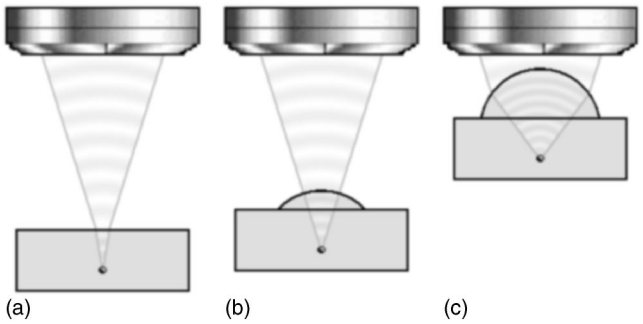

FIG. 2. Imaging a subsurface structure in an object with (a) a conventional optical microscope, (b) a central NAIL, and (c) an aplanatic NAIL.

As illustrated in Figs. 2(b) and 2(c), the addition of a NAIL, a plano-convex lens, to the planar surface of an object increases the conventional optical microscope's light-gathering and resolving power from that object, without introducing any aberrations.[25] When first proposed and demonstrated, the NAIL was termed a truncated SIL; however, the terms SIL and NAIL were later adopted to delineate between application of a plano-convex lens for surface and subsurface microscopy, respectively.[2,26] In surface microscopy with a SIL, the refractive index in the object space is altered by immersion. In subsurface microscopy, the refractive index in the object space may be high, but cannot be altered since the optical near-field of the object is not accessible, thus a NAIL simply increases the NA or light-gathering power. Increasing the NA, which is ultimately limited to n, improves the spatial resolution, which is ultimately limited to $\approx\lambda_0/2n$ laterally

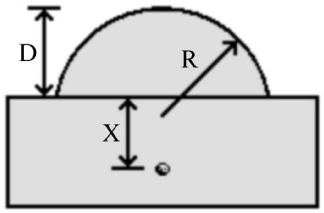

FIG. 3. Parameters of the object and NAIL.

and $\approx\lambda_0/n$ longitudinally. Preferably, the NAIL is made of a material with a refractive index matching that of the encapsulating medium. The planar surface of the NAIL closely matches that of the object, so that light propagates from the object into the NAIL by evanescently coupling across any potential finite gap between them. After propagating through the NAIL, the light then refracts at the spherical surface into air and is collected by a conventional optical microscope. A general set of experimental procedures for using a NAIL in a conventional optical microscope is described by Ippolito.[27]

The key parameters of the object and NAIL are shown in Fig. 3. The subsurface structure within the object to be imaged is located at a depth of X below the planar surface of the object. The convex surface of the NAIL is spherical with a radius of curvature of R. The center thickness of the NAIL, the distance from the top of the spherical surface to the planar surface, is D. There are two types of NAILs that create stigmatic or aberration-free images. A central NAIL, as illustrated in Fig. 2(b), is designed to have the subsurface structures in an object at the geometrical center of the spherical surface of the NAIL, so D must equal $R-X$. An aplanatic NAIL, as illustrated in Fig. 2(c), is designed to have the subsurface structures in an object at the aplanatic points of the spherical surface of the NAIL, so D must equal $R(1+1/n)-X$.[28] Similarly, there are two types of SILs that create stigmatic images. A central SIL, which is usually referred to as a hemispherical SIL, is designed to have the surface of an object at the geometrical center of the spherical surface of the SIL, so D must equal R. An aplanatic SIL, which is usually referred to as a Weierstrass or hyper-hemispherical SIL, is designed to have the subsurface structures in an object at the aplanatic points of the spherical surface of the SIL, so D must equal $R(1+1/n)$.

II. THEORETICAL OPTICAL MODELING

In this section, a theoretical optical model for imaging subsurface structures in an object with a planar surface, both without and with a NAIL, will be described and the results will be compared. The principles of electromagnetic optics will be used to characterize the behavior of light at the surfaces of the object and NAIL, as well as at the focus in the object space. For mathematical simplicity the principles of geometrical optics will be used to characterize the behavior of light in the remaining areas of the object and NAIL. Two approximations are made in the theoretical optical model. The first approximation is that the object space consists of a homogeneous medium, even though a subsurface structure may be present. The second approximation is that the reflections from the surfaces of the object and NAIL do not significantly contribute to the electromagnetic fields at the focus in the object space. In order to present an example in addition to the general model, numerical values will be calculated for near-infrared inspection microscopy of a Si IC, both without and with a Si NAIL, at a λ_0 of 1.3 μm, where the refractive index of Si is 3.5.

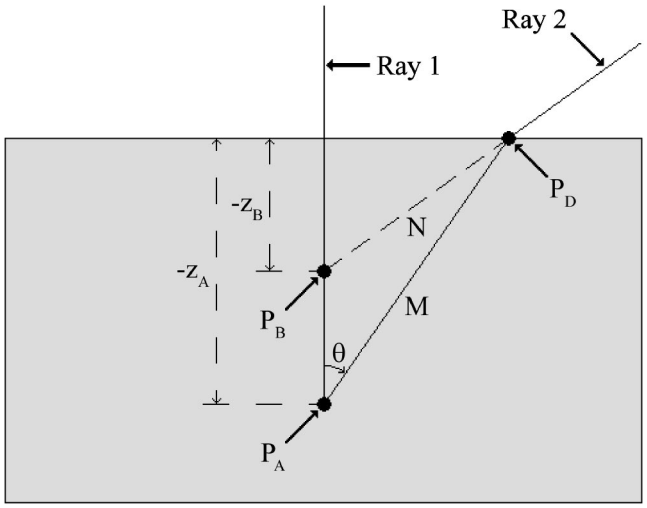

FIG. 4. Imaging parameters for an object with a planar surface.

A. Imaging subsurface structures without a NAIL

A theoretical optical model for imaging subsurface structures in an object with a planar surface, without a NAIL, will be presented beginning with the Gaussian optics approximation of imaging. The planar dielectric boundary between the object, with a refractive index of n, and air, with a refractive index of unity, passes through the origin. The lateral location of the origin is arbitrary, because of the stratified nature of the object along the longitudinal direction. As illustrated in Fig. 4, an object point $\mathbf{P}_A$ with cylindrical coordinates (ρ_A, φ_A, z_A) is imaged by refraction to a virtual image point $\mathbf{P}_B$ with cylindrical coordinates (ρ_B, φ_B, z_B). Within the realm of Gaussian optics, ρ_B is equal to ρ_A, φ_B is equal to φ_A, and z_B is equal to z_A/n. The lateral magnification is equal to unity and the longitudinal magnification is equal to $1/n$. The primary longitudinal chromatic aberration, the longitudinal displacement of the object point to first order due to the change in refractive index dn of the dispersive object, is equal to $z_A dn/n$.

The geometrical aberrations that become significant as θ increases will now be found. Ray 1, shown in Fig. 4, originates from $\mathbf{P}_A$, passes through $\mathbf{P}_B$, and is parallel to the optical axis, which is the z axis. Ray 1 is defined as the reference ray, and the exit pupil is defined as the planar surface of the object. Ray 2 originates from $\mathbf{P}_A$, intersects the planar boundary at $\mathbf{P}_D$, and has a direction in the object space defined in spherical coordinates (θ, ψ). The distances from $\mathbf{P}_A$ to $\mathbf{P}_D$ and $\mathbf{P}_B$ to $\mathbf{P}_D$ are defined as M and N, given in Eqs. (1) and (2), respectively. The optical path length (OPL) from $\mathbf{P}_A$ to $\mathbf{P}_D$ and back to $\mathbf{P}_B$ is given in Eq. (3), and the resulting wave aberration function Φ is given in Eq. (4). The wave aberration function is independent of ρ_A, φ_A, and ψ, because of the planar geometry, so only spherical aberration propor-

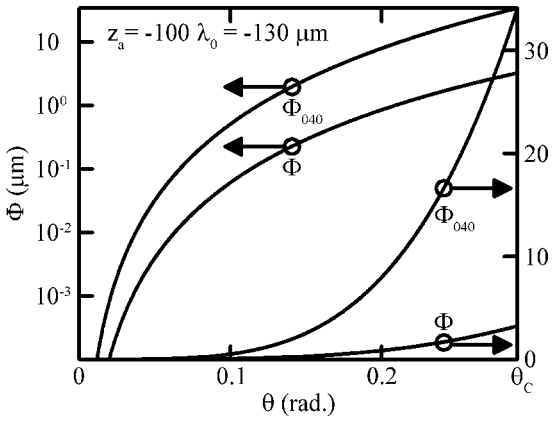

FIG. 5. Wave aberration functions, as function of θ.

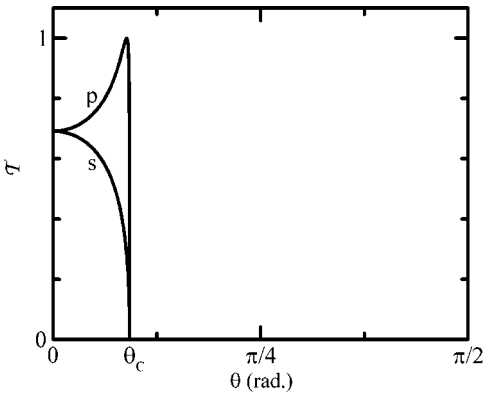

FIG. 6. Transmissivity $\mathcal{T}$, as a function of θ.

tional to z_A is present. The primary spherical aberration Φ_{040} term in the power series expansion of the wave aberration function, as a function of sin θ, is given in Eq. (5). Figure 5 shows the wave aberration function, and primary spherical aberration at z_A equals 130 μm, in Si at a λ_0 of 1.3 μm, on both logarithmic and linear scales, as a function of θ, up to the critical angle θ_c of 0.29 rad. Figure 5 clearly demonstrates that the primary spherical aberration is not a good estimate for the wave aberration function in this angular domain,[29]

$$M = \frac{-z_A}{\cos\theta}, \tag{1}$$

$$N = \sqrt{z_B^2 - z_A^2 + M^2}, \tag{2}$$

$$\mathrm{OPL}_{(z_A,\theta)} = nM - N = \frac{-z_A}{\cos\theta}\left[n - \sqrt{\cos^2\theta\left(\frac{1}{n^2} - 1\right) + 1}\right], \tag{3}$$

$$\Phi = \mathrm{OPL}_{(z_A,\theta)} - \mathrm{OPL}_{(z_A,0)} = z_A\left\{n - \frac{1}{n} - \frac{1}{\cos\theta}\left[n - \sqrt{\cos^2\theta\left(\frac{1}{n^2} - 1\right) + 1}\right]\right\}, \tag{4}$$

$$\Phi_{040} = -z_A\frac{n}{8}(n^2 - 1)\sin^4\theta. \tag{5}$$

The transmission coefficients (t_s and t_p) and the resulting transmissivities for refraction at the planar surface of the object, where the angle of incidence is θ, are given by the Fresnel formulae.[28] Figure 6 shows the transmissivity $\mathcal{T}$ for s and p polarized light in Si at a λ_0 of 1.3 μm, as a function of θ. For a uniform emitter, which has a constant intensity per unit solid angle, total internal reflection above the critical angle greatly reduces the amount of light collected. The collection efficiency (CE) is equal to the ratio of the power transmitted into air P_t to the power incident on the planar boundary of the object P_i. Equation (6) integrates the transmissivities to yield the collection efficiency for a uniform emitter of unpolarized light in the object space. Assuming a full $\pi/2$ angular semiaperture, for Si at a λ_0 of 1.3 μm the collection efficiency is 0.03, which leaves significant room for improvement by a NAIL,

$$\mathrm{CE} = \frac{P_t}{P_i} = \frac{1}{2}\int_0^{\theta_a} (\mathcal{T}_s + \mathcal{T}_p)\sin(\theta)d\theta. \tag{6}$$

Consideration of a high angular semiaperture beam focused at the origin in the object space requires a model of diffraction defined by vector field theory, rather than scalar field theory.[30] An angular spectrum of plane waves method, as described by Wolf, can be used to find the electromagnetic fields at any point near the focus, with cylindrical coordinates (ρ, φ, z).[31] Ichimura *et al.* formulated the electromagnetic fields for an optical system, consisting of a SIL and a magneto-optical disk, based on a formulation for an aplanatic system by Richards and Wolf.[26,32] Parts of the Wolf and Ichimura formulations are used to construct the following formulation, in which the illumination is uniform, the polarization cross terms are equal to zero, and an additional phase change of $k_0\Phi$ is introduced to account for the geometrical aberrations. The resulting complex amplitudes (**E** and **H**) are given by Eqs. (7)–(11). The resulting time-averaged Poynting vector $\langle S\rangle$ and the intensity $|\langle S\rangle|$ are given in Eqs. (12) and (13), respectively. In this model, the incident beam is polarized; however, if unpolarized light is considered the intensity will be the same,

$$\mathbf{E} = E_0\begin{pmatrix} -i[I_0 + I_2\cos(2\varphi)] \\ -iI_2\sin(2\varphi) \\ -2I_1\cos(\varphi) \end{pmatrix}, \tag{7}$$

$$\mathbf{H} = \frac{E_0}{\eta}\begin{pmatrix} -iI_2\sin(2\varphi) \\ -i[I_0 - I_2\cos(2\varphi)] \\ -2I_1\sin(\varphi) \end{pmatrix}, \tag{8}$$

$$I_0 = \int_0^{\theta_a} (t_s + t_p\cos\theta)\sin\theta J_0(nk_0\rho\sin\theta)e^{ink_0 z\cos\theta + ik_0\Phi}d\theta, \tag{9}$$

$$I_1 = \int_0^{\theta_a} t_p\sin^2\theta J_1(nk_0\rho\sin\theta)e^{ink_0 z\cos\theta + ik_0\Phi}d\theta, \tag{10}$$

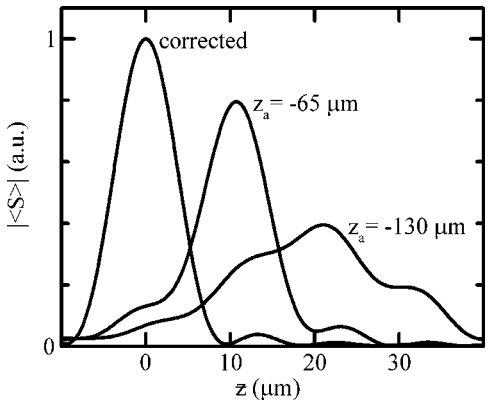

FIG. 7. Intensity along the optical axis at ρ equals zero, as a function of z.

$$I_2 = \int_0^{\theta_a} (t_s - t_p \cos\theta) \sin\theta J_2(nk_0\rho \sin\theta) e^{ink_0 z \cos\theta + ik_0\Phi} d\theta, \tag{11}$$

$$\langle S \rangle = \frac{1}{2}\mathrm{Re}\{\mathbf{E} \times \mathbf{H}^*\} = \frac{E_0^2}{2\eta}\begin{pmatrix} 2\cos(\varphi)\mathrm{Im}[I_1^*(I_0 - I_2)] \\ 2\sin(\varphi)\mathrm{Im}[I_1^*(I_0 - I_2)] \\ |I_0|^2 - |I_2|^2 \end{pmatrix}, \tag{12}$$

$$|\langle S \rangle| = \frac{E_0^2}{2\eta}\sqrt{(|I_0|^2 - |I_2|^2)^2 + 4\{\mathrm{Im}[I_1^*(I_0 - I_2)]\}^2}. \tag{13}$$

Using this vector field formulation, the intensity is calculated in the vicinity of $\mathbf{P}_A$, for several values of z_A in Si at a λ_0 of 1.3 μm. We assume the illumination of $\mathbf{P}_B$ is unpolarized and uniform, and the angular semiaperture is θ_c. The wave aberration function Φ for this geometry was given in Eq. (4), and the focus coordinate z is equal to $z_A - z$. Figure 7 shows the intensity along the optical axis at ρ equals zero, as a function of z. Figure 8 shows the intensity in the lateral plane of peak intensity, as a function of ρ. Table I shows the imaging characteristics at several values of z_A. The spatial resolution is defined as the full-width-at-half maximum of the intensity, according to the Houston criterion.[33] The Strehl ratio is the ratio of the maximum intensities, with and without aberrations. If the Strehl ratio is greater than or equal to 0.8, the spatial resolution is said to be diffraction limited.[28]

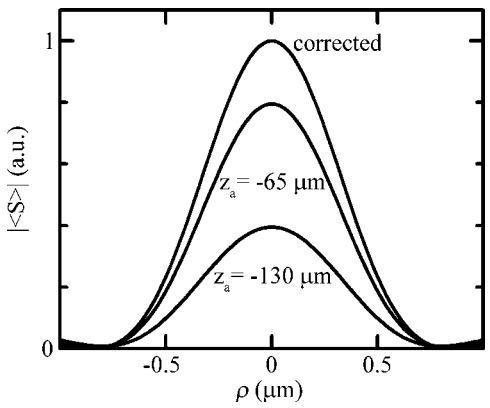

FIG. 8. Intensity in the lateral plane of peak intensity, as a function of ρ.

TABLE I. Imaging characteristics without a NAIL at several values of z_A.

		Spatial resolution	
z_A (μm)	Strehl ratio	Lateral (μm)	Longitudinal (μm)
Corrected	1	0.71	8.4
−65	0.80	0.72	9.1
−130	0.40	0.73	19.7
−260	0.19	0.96	52.7
−520	0.09	1.28	119

For the most practical depths of greater than 65 μm in Si at a λ_0 of 1.3 μm, the spherical aberration must be corrected by the objective lens or elsewhere, to operate at diffraction limited spatial resolution. To achieve these values of spatial resolution and collection efficiency would require an objective lens with a NA of unity, so in practice the values are significantly degraded. Rigorous analytical modeling and numerical simulation of light, focused through a planar dielectric boundary, were previously conducted by Török *et al.*.[34–36]

B. Imaging subsurface structures with a NAIL

We now describe a theoretical optical model for imaging subsurface structures in an object with a planar surface using a NAIL. A geometrical optics model of a sphere, with a refractive index of n, in air, with a refractive index of unity, will be used to model to the object and NAIL. As illustrated in Fig. 9, the dielectric boundary between the sphere and air

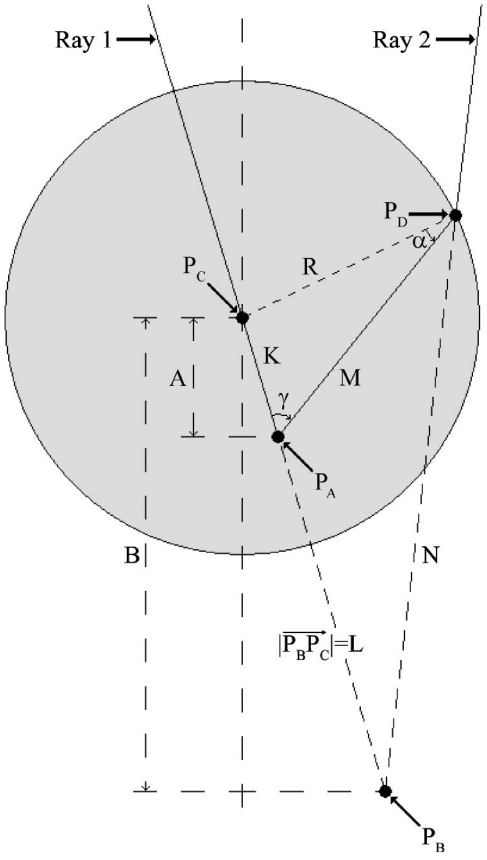

FIG. 9. Imaging parameters for a sphere.

has a radius of curvature of R and is centered at the origin $\mathbf{P}_C$. An object point $\mathbf{P}_A$ with cylindrical coordinates $(\rho_A, \varphi_A, -A)$ is imaged by refraction to a virtual image point $\mathbf{P}_B$ with cylindrical coordinates $(\rho_B, \varphi_B, -B)$, according to Eqs. (14)–(18), within the realm of Gaussian optics.

$$B = \frac{n}{\frac{A}{R}(1-n)+1}A, \tag{14}$$

$$\rho_B = \frac{n}{\frac{A}{R}(1-n)+1}\rho_A, \tag{15}$$

$$\varphi_B = \varphi_A, \tag{16}$$

$$\textit{lateral magnification} = \frac{n}{\frac{A}{R}(1-n)+1}, \tag{17}$$

$$\textit{longitudinal magnification} = \frac{n}{\left(\frac{A}{R}(1-n)+1\right)^2}. \tag{18}$$

Next, the geometrical aberrations that become significant, as θ increases, are found. Ray 1, shown in Fig. 9, originates from $\mathbf{P}_A$, passes through $\mathbf{P}_C$, and is collinear with $\mathbf{P}_B$, in accordance with the projective nature of Eqs. (14)–(16). Ray 1 is defined as the reference ray, and the exit pupil is defined as the surface of the sphere. Ray 2 originates from $\mathbf{P}_A$, intersects the spherical boundary at $\mathbf{P}_D$, and has a direction in the object space defined in spherical coordinates (θ, ψ). Ray 2 forms an angle of γ, with respect to Ray 1, and an angle of α, with respect to the line from $\mathbf{P}_C$ to $\mathbf{P}_D$. The distances from $\mathbf{P}_A$ to $\mathbf{P}_C$ and $\mathbf{P}_B$ to $\mathbf{P}_C$ are defined as K and L, respectively. The distances from $\mathbf{P}_A$ to $\mathbf{P}_D$ and $\mathbf{P}_B$ to $\mathbf{P}_D$ are defined as M and N, given in Eqs. (19) and (20), respectively. The optical path length from $\mathbf{P}_A$ to $\mathbf{P}_D$ and back to $\mathbf{P}_B$ is given in Eq. (21), and the resulting wave aberration function is given in Eq. (22),

$$M = K\cos(\gamma) + \sqrt{R^2 - K^2\sin^2(\gamma)}, \tag{19}$$

$$N = \sqrt{R^2 + L^2 + 2L(M\cos(\gamma) - K)}, \tag{20}$$

$$\mathrm{OPL}_{(K,L,\gamma)} = nM - N = nK\cos(\gamma) + n\sqrt{R^2 - K^2\sin^2(\gamma)} - \sqrt{R^2 + L^2 + 2L[-K\sin^2(\gamma) + \cos(\gamma)\sqrt{R^2 - K^2\sin^2(\gamma)}]}, \tag{21}$$

$$\Phi = \mathrm{OPL}_{(K,L,\gamma)} - \mathrm{OPL}_{(K,L,0)} = R(1-n) + nK[\cos(\gamma) - 1] + L + n\sqrt{R^2 - K^2\sin^2(\gamma)} - \sqrt{R^2 + L^2 + 2L[-K\sin^2(\gamma) + \cos(\gamma)\sqrt{R^2 - K^2\sin^2(\gamma)}]}. \tag{22}$$

So far, the wave aberration function has been derived purely from geometry, and the Gaussian optics relationships between K and L, Eqs. (14)–(16), have not been applied. This was done to show that there are two solutions for K and L, where the wave aberration function is equal to zero for all γ, and therefore the imaging is stigmatic. In the central solution, both K and L are equal to zero, which occurs when both $\mathbf{P}_A$ and $\mathbf{P}_B$ are at $\mathbf{P}_C$. For the central solution, the rays are normal to the spherical boundary, and refraction does not change their direction. In the aplanatic solution, K and L are equal to R/n and Rn, respectively, and as previously mentioned, $\mathbf{P}_A, \mathbf{P}_B$, and $\mathbf{P}_C$ are collinear. The points on the spherical surface, defined by K equal to R/n in the aplanatic solution, are termed the aplanatic points of the spherical boundary. The Gaussian optics relationships between K and L, Eqs. (14)–(16), yield the values for K, L, γ, and α given by Eqs. (23)–(25), respectively, in terms of the object point and Ray 2 coordinates,

$$K = \sqrt{A^2 + \rho_A^2}, \tag{23}$$

$$L = \frac{n}{\frac{A}{R}(1-n)+1}\sqrt{A^2 + \rho_A^2}, \tag{24}$$

$$\cos\gamma = \frac{-\rho_A\sin\theta\cos(\varphi_A - \psi) + A\cos\theta}{\sqrt{A^2 + \rho_A^2}}, \tag{25}$$

$$\sin\alpha = \frac{\sin\gamma\sqrt{A^2 + \rho_A^2}}{R}. \tag{26}$$

The geometrical optics model of the sphere in air can be extended to the object and NAIL by including three additional effects. The first effect is the transmission for refraction at the spherical surface of the NAIL, which is governed by the Fresnel formulas. The second effect is the transmission across an air gap that exists in practice between the object and NAIL. The object, air gap, and NAIL are modeled as a stratified medium consisting of; a gap layer with a thickness of h and a refractive index of unity for air, between two bulk layers with a refractive index of n for the object and NAIL. The characteristic matrix method is then used to solve for the transmission coefficients and the resulting transmissivities and phase changes on transmission.[28] Figure 10 shows the transmissivity and phase change on transmission δ_t for s and p polarized light across an air gap between a Si object and NAIL at a λ_0 of 1.3 μm, as a function of θ. Simulations for the transmission across an air gap between an object and a SIL, in the visible spectrum, were previously conducted by Milster *et al.*.[37,38] The transmission coefficients for refraction at the spherical surface of the NAIL and the transmission coefficients across an air gap between the object and NAIL can be multiplied, to yield the total transmission coefficients of t_s and t_p, for points along the optical axis,

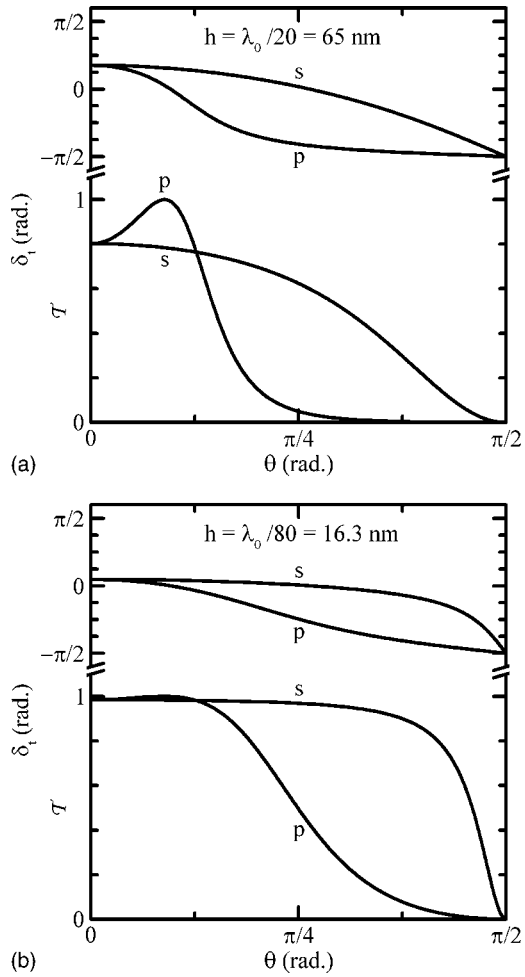

FIG. 10. Transmissivity $\mathcal{T}$ and phase change on transmission δ_t, as a function of θ, for an air gap height h of (a) $\lambda_0/20$ and (b) $\lambda_0/80$.

because the planes of incidence for both refractions are the same. The third effect is the angular semiaperture defined by the region of optical contact between the object and NAIL. If the planar surface of the object extends beyond the planar surface of the NAIL, as shown in Fig. 3, the angular semiaperture is given by Eq. (27),

$$\sin\theta_a = \left(\frac{X^2}{R^2-(X-A)^2}+1\right)^{-1/2}. \tag{27}$$

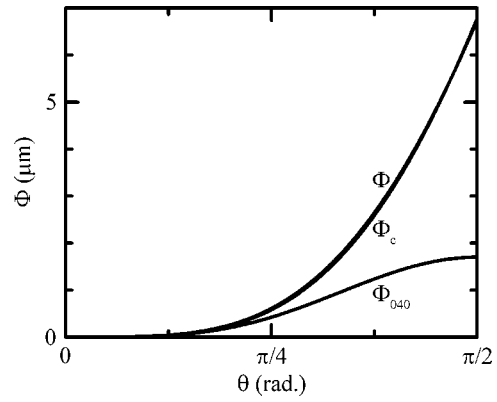

FIG. 11. Wave aberration functions, as function of θ.

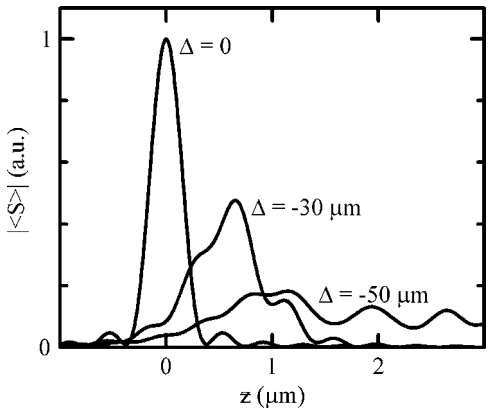

FIG. 12. Intensity along the optical axis at ρ equals zero, as a function of z.

1. Central NAIL

The central NAIL is based on the central stigmatic solution, where A and B are both equal to zero, so D must equal $R-X$. For a central NAIL, R should be selected to be less than the working distance of the objective lens. The lateral and longitudinal magnifications are both equal to n. The primary longitudinal chromatic aberration is equal to zero. According to Eq. (26), if A and ρ_A are much smaller than R, then α is approximately equal to zero. Thus, the transmission coefficient and the resulting transmissivity for refraction at the spherical surface of the central NAIL, where the angle of incidence is α, are given by the Fresnel formula for normal incidence.[28] Assuming a full $\pi/2$ angular semiaperture and no air gap, for Si at a λ_0 of 1.3 μm the collection efficiency is 0.69.

At the central stigmatic solution, the only primary aberrations are astigmatism and distortion. The variable Δ will be the longitudinal displacement from the stigmatic solution, so for the central NAIL, A is equal to Δ. The first term Φc in the power series expansion of the wave aberration function along the optical axis around the central stigmatic solution, as a function of Δ, is given in Eq. (28), which is equivalent to the expression given by Baba *et al.*.[10] Again, in this angular domain the primary spherical aberration Φ_{040}, given in Eq. (29), is not a good estimate for the wave aberration function.[29] These wave aberration functions are shown in Fig. 11 for a central NAIL with R equal to 1.61 mm and Δ

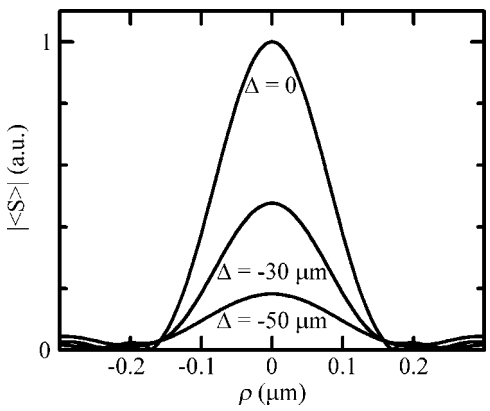

FIG. 13. Intensity in the lateral plane of peak intensity, as a function of ρ.

TABLE II. Imaging characteristics with a central NAIL for varying longitudinal displacement from the stigmatic solution Δ.

		Spatial resolution	
Δ (μm)	Strehl ratio	Lateral (μm)	Longitudinal (μm)
0	1	0.17	0.34
−22	0.80	0.17	0.36
−30	0.48	0.18	0.66
−32	0.40	0.18	0.73
−40	0.29	0.20	1.41
−50	0.18	0.21	2.40
−60	0.14	0.23	3.74

equal to −50 μm. The wave aberration functions, Φ and Φ_c, are approximately the same at this value of Δ,

$$\Phi_c = 2n(n-1)\frac{\Delta^2}{R}\sin^4\left(\frac{\theta}{2}\right), \tag{28}$$

$$\Phi_{040} = n(n-1)\frac{\Delta^2}{8R}\sin^4\theta. \tag{29}$$

The intensity, using a central NAIL with R equal to 1.61 mm, is calculated in the vicinity of $\mathbf{P}_A$ for several values of Δ, in Si at a λ_0 of 1.3 μm. We assume the illumination of $\mathbf{P}_B$ is unpolarized and uniform, the angular semiaperture is a full $\pi/2$, and no air gap exists. The wave aberration function was given in Eq. (22), and the focus coordinate z is equal to $-\Delta - z$. Figure 12 shows the intensity along the optical axis at ρ equals zero, as a function of z. Figure 13 shows the intensity in the lateral plane of peak intensity, as a function of ρ. Table II shows the imaging characteristics at several values of Δ. Thus, the absolute value of Δ must be less than 22 μm to operate at diffraction limited spatial resolution. However, significant gains in spatial resolution still exist, as the Strehl ratio is equal to 0.4 when Δ is equal to 32 μm. To achieve these values of spatial resolution and collection efficiency would require an objective lens with a NA of unity, so in practice the values are significantly degraded.

2. Aplanatic NAIL

The aplanatic NAIL is based on the aplanatic stigmatic solution, where A and B are equal to R/n and Rn, respectively, so D must equal $R(1+1/n)-X$. For an aplanatic NAIL, R should be selected such that $R(n+1)$ is less than the working distance of the objective lens. The lateral and longitudinal magnifications are equal to n^2 and n^3, respectively. The primary longitudinal chromatic aberration is equal to $R(n+1)dn/n^3$. According to Eqs. (25) and (26), if A is equal to R/n and ρ_A is much smaller than A, then γ and $\sin\alpha$ are approximately equal to θ and $\sin\theta/n$, respectively. The transmission coefficients and the resulting transmissivity for refraction at the spherical surface of the aplanatic NAIL, where the angle of incidence is α, are given by the Fresnel formulas. Figure 14 shows the transmissivity for refraction at the spherical surface of the NAIL for s and p polarized light in Si at a λ_0 of 1.3 μm, as a function of θ. Assuming a full $\pi/2$ angular semiaperture and no air gap, for Si at a λ_0 of 1.3 μm the collection efficiency is 0.62.

At the aplanatic stigmatic solution, the only primary aberrations are curvature of field and distortion. Again, Δ is the longitudinal displacement from the stigmatic solution, so for the aplanatic NAIL, A is equal to $R/n+\Delta$. The first term Φ_a in the power series expansion of the wave aberration function along the optical axis around the aplanatic stigmatic solution, as a function of Δ, is given in Eq. (30). As shown in Fig. 15, the wave aberration functions, Φ and Φ_a, for an aplanatic NAIL with R equal to 1.61 mm and Δ equal to −8 μm, are approximately the same,

$$\Phi_a = n\Delta(\cos\theta - 1 + n^2 - n\sqrt{n^2 - \sin^2\theta}). \tag{30}$$

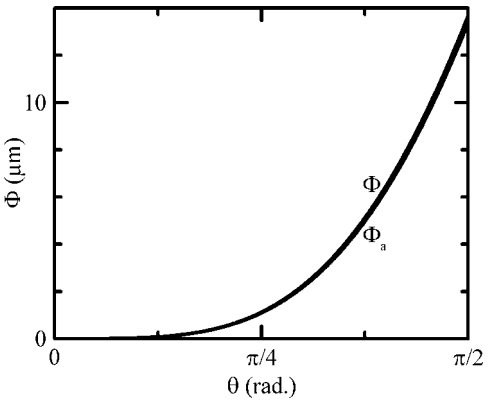

FIG. 15. Wave aberration functions, as function of θ.

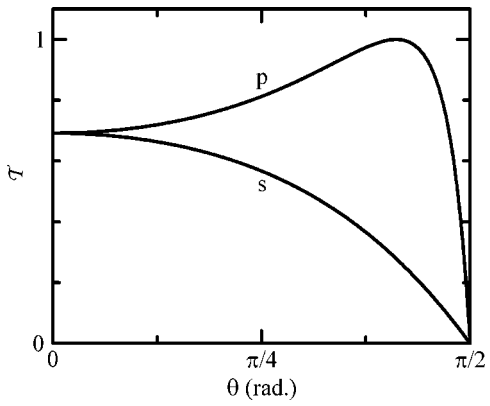

FIG. 14. Transmissivity $\mathcal{T}$, as a function of θ.

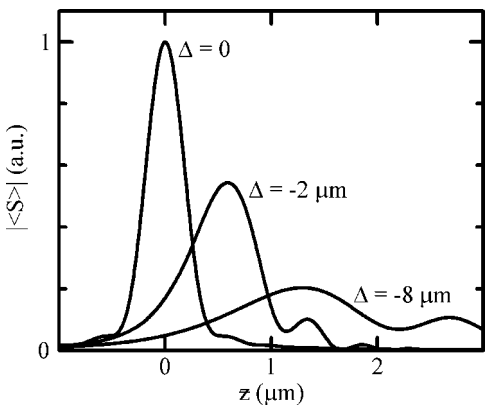

FIG. 16. Intensity along the optical axis at ρ equals zero, as a function of z.

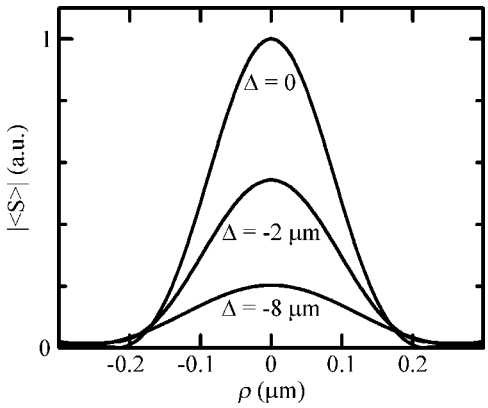

FIG. 17. Intensity in the lateral plane of peak intensity, as a function of ρ

.

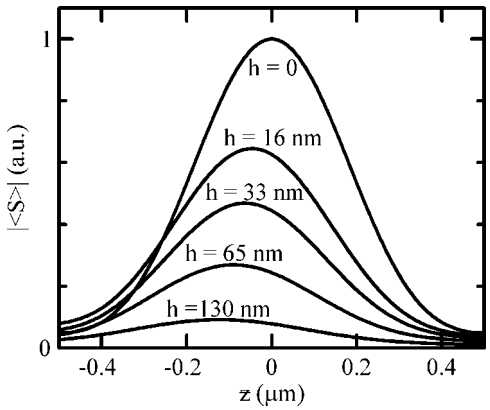

FIG. 18. Intensity along the optical axis at ρ equals zero, as a function of z

.

The intensity, using an aplanatic NAIL with R equal to 1.61 mm, is calculated in the vicinity of $\mathbf{P}_A$ for several values of Δ, in Si at a λ_0 of 1.3 μm. We assume the illumination of $\mathbf{P}_B$ is unpolarized and uniform, the angular semiaperture is a full $\pi/2$, and no air gap exists. The wave aberration function was given in Eq. (22), and the focus coordinate z is equal to $-R/n-\Delta-z$. Figure 16 shows the intensity along the optical axis at ρ equals zero, as a function of z. Figure 17 shows the intensity in the lateral plane of peak intensity, as a function of ρ. Table III shows the imaging characteristics at several values of Δ. Thus, the absolute value of Δ must be less than 1 μm to operate at diffraction limited spatial resolution. However, significant gains in spatial resolution still exist, as the Strehl ratio is equal to 0.4 when Δ is equal to 3.2 μm. To achieve these values of spatial resolution and collection efficiency requires an objective lens with a NA of $1/n$, which is usually available in practice.

The intensity, using an aplanatic NAIL with R equal to 1.61 mm, is calculated in the vicinity of $\mathbf{P}_A$ for several values of air gap height h, in Si at a λ_0 of 1.3 μm. We assume the illumination of $\mathbf{P}_B$ is unpolarized and uniform, and the angular semiaperture is a full $\pi/2$. We assume the focus is at the aplanatic stigmatic solution, so Δ and the wave aberration function are equal to zero, and the focus coordinate z is equal to $-R/n-z$. Figure 18 shows the intensity along the optical axis at ρ equals zero, as a function of z. Figure 19 shows the intensity in the lateral plane of peak intensity, as a function of ρ. Table IV shows the imaging characteristics at several values of air gap height h, including the resulting changes in collection efficiency, as defined by Eq. (6), for Si at a λ_0 of 1.3 μm. Thus, the air gap height must be less than 7.8 nm to operate at diffraction limited spatial resolution. However, significant gains in spatial resolution still exist, as the Strehl ratio is equal to 0.4 when the air gap height is equal to 41 nm.

TABLE III. Imaging characteristics with an aplanatic NAIL for varying longitudinal displacement from the stigmatic solution Δ.

		Spatial resolution	
Δ (μm)	Strehl ratio	Lateral (μm)	Longitudinal (μm)
0	1	0.19	0.42
−1	0.80	0.20	0.51
−2	0.54	0.21	0.73
−3.2	0.40	0.22	0.92
−4	0.34	0.2	1.02
−8	0.20	0.26	2.30
−16	0.12	0.30	3.33

C. Comparison of theoretical results

The theoretical optical models for imaging subsurface structures in an object with a planar surface, both with and without a NAIL, will now be compared. Numerical values, assuming there is no air gap, will also be compared for near-infrared inspection microscopy, two other Si IC failure analysis applications, spectroscopy of single quantum dots, and optical data storage. Again, in the first example of near-infrared inspection microscopy of a Si IC at a λ_0 of 1.3 μm, the refractive index of Si is 3.5. Numerical values are calculated for a 0.5 mm thick Si IC, both without and with a Si NAIL having R equal to 1.61 mm.[25] The second example is thermal emission microscopy of a 1 mm thick Si IC, using an InSb detector, both without and with a Si NAIL having R equal to 1.61 mm.[39] In this example, most of the light is at free space wavelengths between 4 μm and 5 μm, where the refractive index of Si monotonically varies from 3.4294 to 3.4261, respectively. The third example is picosecond imag-

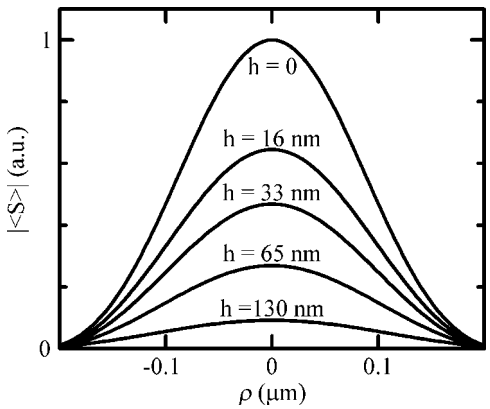

FIG. 19. Intensity in the lateral plane of peak intensity, as a function of ρ.

TABLE IV. Imaging characteristics with an aplanatic NAIL for varying air gap height h.

h	h (nm)	Strehl ratio	Spatial resolution Lateral (μm)	Spatial resolution Longitudinal (μm)	Collection efficiency
	0	1	0.19	0.42	0.62
$\lambda_0/166$	7.8	0.80	0.20	0.44	0.40
$\lambda_0/80$	16.3	0.65	0.20	0.44	0.32
$\lambda_0/40$	32.5	0.47	0.21	0.45	0.24
$\lambda_0/31$	41.4	0.40	0.21	0.46	0.21
$\lambda_0/20$	65	0.27	0.22	0.48	0.16
$\lambda_0/10$	130	0.09	0.23	0.53	0.07
$\lambda_0/6$	217	0.026	0.27	0.68	0.03
$\lambda_0/4$	325	0.008	0.35	2.57	0.02

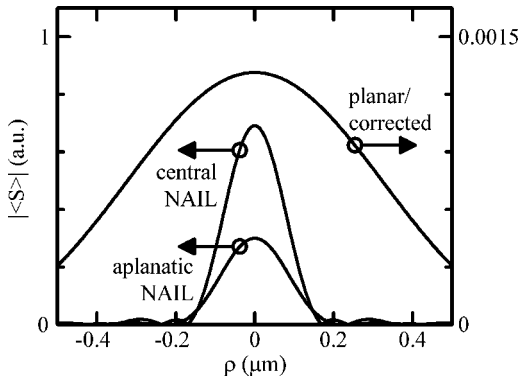

FIG. 20. Intensity in the object plane at z equals zero, as a function of ρ

.

ing circuit analysis (PICA) of a 0.1 mm thick Si IC, using an InGaAs avalanche photodiode or a superconducting single-photon detector, both without and with a Si NAIL having R equal to 0.4 mm.[40–42] In this example, most of the light is at free space wavelengths between 1.2 μm and 1.53 μm, where the refractive index of Si monotonically varies from 3.519 to 3.478, respectively. The fourth example is photoluminescence microscopy of individual InGaAs quantum dots on a 0.5 mm thick GaAs substrate, both without and with a GaAs NAIL having R equal to 1.61 mm.[43] In this example, a spectrum is acquired between the free space wavelengths of 0.94 μm and 0.96 μm, where the refractive index of GaAs monotonically varies from 3.489 to 3.475, respectively. The fifth example is optical data storage on a Blu-ray Disc at a λ_0 of 405 nm, where the refractive index of the 0.1 mm thick cover layer on the disc is 1.5, both without and with a glass NAIL having R equal to 0.2 mm and a matching refractive index equal to 1.5.[29]

The calculated lateral and longitudinal spatial resolution values for each example, both without and with an aplanatic NAIL and a central NAIL, are shown in Table V and compare well to the approximations for the ultimate limit on spatial resolution due to the diffraction of light. Note that to achieve the stated values of spatial resolution for conventional subsurface microscopy requires an objective lens that corrects for the spherical aberration introduced by refraction at the planar surface of the object. For comparison in Si at a λ_0 of 1.3 μm, assuming a full $\pi/2$ angular semiaperture, Fig. 20 shows the intensity in the object plane at z equals to zero, as a function of ρ, and Fig. 21 shows the intensity along the optical axis at ρ equals zero, as a function of z. The intensity for conventional subsurface microscopy (planar/corrected) has to be placed on a separate scale because the light-gathering power is so low. The lateral and longitudinal spatial resolution improvements resulting from the NAIL are approximately factors of n and $n^2(1+\cos\theta_c)$, which are 3.5 and 24, respectively, in Si at a λ_0 of 1.3 μm. The effective volume of the focus is reduced by a factor of $\approx n^4(1+\cos\theta_c)$, which in Si at a λ_0 of 1.3 μm is 294. The calculated collection efficiency values for selected examples, as defined by Eq. (6), are shown in Table VI. In the example of near-infrared inspection microscopy, the improvement in collection efficiency is approximately a factor of 10. To achieve the stated values of spatial resolution and collection efficiency with a conventional optical microscope, both without and with a central NAIL, would require an objective lens with a NA of unity; so in practice, the values will be significantly degraded. However, the stated values of spatial resolution and collection efficiency can be achieved in practice with an aplanatic NAIL and an objective lens with a NA of $1/n$.

A further advantage of using a NAIL is the additional lateral and longitudinal magnification it provides, as shown in Table VII for selected examples. If the object and NAIL are affixed to each other, then the additional magnification greatly reduces the positioning noise due to vibration and drift, and causes a scan relaxation that allows less accurate, and therefore less costly, scanning stages to be used for positioning of the object and NAIL. Another advantage of using a NAIL is a reduction in longitudinal chromatic aberration, as shown in Table VIII. For polychromatic applications

TABLE V. Comparison of lateral and longitudinal spatial resolution.

	Corrected conventional		Aplanatic NAIL		Central NAIL	
	Lateral (μm)	Longitudinal (μm)	Lateral (μm)	Longitudinal (μm)	Lateral (μm)	Longitudinal (μm)
Approximation	$\lambda_0/2$	$\lambda_0 n(1+\cos\theta_c)$	$\lambda_0/2n$	λ_0/n	$\lambda_0/2n$	λ_0/n
Near-infrared inspection	0.71	8.40	0.20	0.49	0.19	0.88
Thermal emission	2.74	31.6	0.90	2.92	0.94	3.42
PICA	0.84	9.81	0.23	0.56	0.22	0.52
Quantum dot	0.53	6.15	0.15	0.37	0.14	0.36
Optical data storage	0.22	1.01	0.15	0.45	0.15	0.48

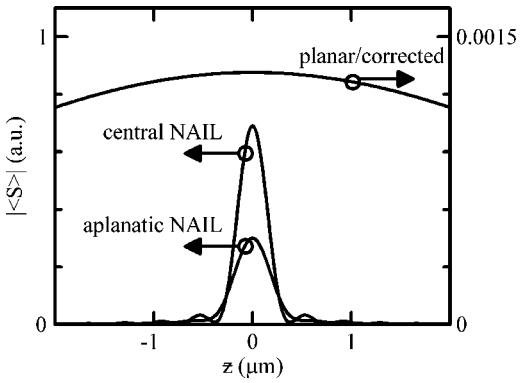

FIG. 21. Intensity along the optical axis at ρ equals zero, as a function of z

.

the central NAIL is often the best choice, because it completely eliminates chromatic aberrations. In PICA measurements, a GaAs or GaP NAIL may be used to reduce the amount of chromatic aberration and absorption caused by a Si NAIL. The theoretical optical modeling indicates that both the central and aplanatic NAILs provide significant improvement in resolving and light-gathering power. Furthermore, improvements in magnification and lower NA requirements for the objective lens provide significant cost savings, when using a NAIL. A choice between the central or aplanatic NAIL should involve consideration of all the contributing factors discussed in this theoretical comparison.

III. CONCLUSIONS

Both the central and aplanatic NAIL have experimentally demonstrated improvements in light-gathering and resolving power that compare well with the results of our theoretical optical modeling. The central NAIL has been used to improve the density of optical data storage at a λ_0 of 546 nm.[29] The theoretical example of optical data storage on a Blu-ray Disc at a λ_0 of 405 nm was presented to show the improvement in density by greater than a factor of 2, available with current technology. The aplanatic NAIL has been used in many applications, but was first demonstrated in near-infrared inspection microscopy of Si IC using a Si NAIL. A lateral spatial resolution of better than 0.23 μm and a longitudinal spatial resolution of better than 1.7 μm were experimentally demonstrated at a λ_0 of 1.05 μm.[25] These experimental spatial resolutions compare well to the theoretical lateral spatial resolution of 0.16 μm and longitudinal spatial resolution of 0.77 μm predicted by modeling. These experimental spatial resolutions represent a significant improvement over the theoretical lateral spatial resolution limit of 0.5 μm and longitudinal spatial resolution limit of 6 μm for corrected conventional subsurface microscopy. In a second experiment, as described in the first theoretical example, a lateral spatial resolution of about 0.3 μm was demonstrated on a commercial near-infrared inspection microscope at a λ_0 of 1.3 μm.[25,27] This experimental lateral spatial resolution is considerably larger than the theoretical lateral spatial resolution of 0.16 μm predicted by modeling, but represents a significant improvement over the theoretical lateral spatial resolution limit of 0.5 μm for corrected conventional subsurface microscopy. The aplanatic NAIL was also experimentally demonstrated in thermal emission microscopy, as described in the second theoretical example. A lateral spatial resolution of 1.4 μm and a longitudinal spatial resolution of 7.4 μm were experimentally demonstrated at free space wavelengths up to 5 μm.[39] These experimental spatial resolutions compare well to the theoretical lateral spatial resolution of 0.90 μm and longitudinal spatial resolution of 2.92 μm predicted by modeling. These experimental spatial resolutions represent a significant improvement over the theoretical lateral spatial resolution limit of 2.74 μm and longitudinal spatial resolution limit of 31.6 μm for corrected conventional subsurface microscopy. The third theoretical example of PICA was given, because we believe a NAIL will soon experimentally yield the great improvements in light-gathering and resolving power as predicted by modeling. An aplanatic Si NAIL has also been used to improve the spatial resolution and amount of light collected in scanning far-infrared microscopy of cyclotron emissions from quantum Hall devices.[44] An aplanatic GaAs NAIL has allowed photoluminescence spectroscopy of an individual InGaAs quantum dot by improving the lateral spatial resolution and increasing the light-gathering power, as described in the fourth theoretical example.[43] These experimental results are currently being prepared for publication. In all of these application examples, the theoretical and experimental results are in good agreement, and we believe NAIL microscopy promises many future improvements in other applications as well.

TABLE VI. Comparison of collection efficiency.

	Conventional	Aplanatic NAIL	Central NAIL
Thermal emission	0.03	0.31	0.27
PICA	0.03	0.52	0.52
Quantum dot	0.03	0.48	0.48

TABLE VII. Comparison of lateral and longitudinal magnification.

	Conventional		Aplanatic NAIL		Central NAIL	
	Lateral	Longitudinal	Lateral	Longitudinal	Lateral	Longitudinal
In general	1	$1/n$	n^2	n^3	n	n
Near-infrared inspection	1	0.29	12.3	42.9	3.5	3.5
Optical data storage	1	0.67	2.25	3.38	1.5	1.5

TABLE VIII. Comparison of primary longitudinal chromatic aberration.

	Conventional (μm)	Aplanatic NAIL (μm)	Central NAIL (μm)
In general	$X\,dn/n$	$R(n+1)dn/n^3$	0
Thermal emission	1.0	0.6	0
PICA	1.2	1.7	0
Quantum dot	2.0	2.4	0

ACKNOWLEDGMENTS

This work was supported by Air Force Office of Scientific Research under Grant No. MURI F-49620-03-1-0379 and by NSF under Grant No. NIRT ECS-0210752. The authors would like to thank Nick Vamivakas for reviewing the manuscript.

[1]C. J. R. Sheppard, J. Microsc. **149**, 73 (1988).
[2]S. M. Mansfield and G. S. Kino, Appl. Phys. Lett. **57**, 2615 (1990).
[3]B. D. Terris, H. J. Mamin, D. Rugar, W. R. Studenmund, and G. S. Kino, Appl. Phys. Lett. **65**, 388 (1994).
[4]B. D. Terris, H. J. Mamin, and D. Rugar, Appl. Phys. Lett. **68**, 141 (1996).
[5]J. A. H. Stotz and M. R. Freeman, Rev. Sci. Instrum. **68**, 4468 (1997).
[6]Q. Wu, R. D. Grober, D. Gammon, and D. S. Katzer, Phys. Rev. Lett. **83**, 2652 (1999).
[7]Q. Wu, R. D. Grober, D. Gammon, and D. S. Katzer, Phys. Rev. B **62**, 13022 (2000).
[8]M. Yoshita, T. Sasaki, M. Baba, and H. Akiyama, Appl. Phys. Lett. **73**, 635 (1998).
[9]M. Yoshita, M. Baba, S. Koshiba, H. Sakaki, and H. Akiyama, Appl. Phys. Lett. **73**, 2965 (1998).
[10]M. Baba, T. Sasaki, M. Yoshita, and H. Akiyama, J. Appl. Phys. **85**, 6923 (1999).
[11]M. Yoshita, N. Kondo, H. Sakaki, M. Baba, and H. Akiyama, Phys. Rev. B **63**, 075305 (2001).
[12]H. Zhao, S. Moehl, S. Wachter, and H. Kalt, Appl. Phys. Lett. **80**, 1391 (2002).
[13]H. Zhao, B. D. Don, S. Moehl, H. Kalt, K. Ohkawa, and D. Hommel, Phys. Rev. B **67**, 035306 (2003).
[14]S. Moehl, H. Zhao, B. D. Don, S. Wachter, and H. Kalt, J. Appl. Phys. **93**, 6265 (2003).
[15]M. Vollmer, H. Giessen, W. Stolz, W. W. Rühle, L. Ghislain, and V. Elings, Appl. Phys. Lett. **74**, 1791 (1999).
[16]Q. Wu, G. D. Feke, R. D. Grober, and L. P. Ghislain, Appl. Phys. Lett. **75**, 4064 (1999).
[17]K. Koyama, M. Yoshita, M. Baba, T. Suemoto, and H. Akiyama, Appl. Phys. Lett. **75**, 1667 (1999).
[18]M. Yoshita, K. Koyama, M. Baba, and H. Akiyama, J. Appl. Phys. **92**, 862 (2002).
[19]C. D. Poweleit, A. Gunther, S. Goodnick, and J. Menéndez, Appl. Phys. Lett. **73**, 2275 (1998).
[20]L. P. Ghislain, V. B. Elings, K. B. Crozier, S. R. Manalis, S. C. Minne, K. Wilder, G. S. Kino, and C. F. Quate, Appl. Phys. Lett. **74**, 501 (1999).
[21]S. Matsuo and H. Misawa, Rev. Sci. Instrum. **73**, 2011 (2002).
[22]D. A. Fletcher, K. B. Crozier, C. F. Quate, G. S. Kino, K. E. Goodson, D. Simanovskii, and D. V. Palanker, Appl. Phys. Lett. **77**, 2109 (2000).
[23]D. A. Fletcher, K. E. Goodson, and G. S. Kino, Opt. Lett. **26**, 399 (2001).
[24]D. A. Fletcher, K. B. Crozier, C. F. Quate, G. S. Kino, K. E. Goodson, D. Simanovskii, and D. V. Palanker, Appl. Phys. Lett. **78**, 3589 (2001).
[25]S. B. Ippolito, B. B. Goldberg, and M. S. Ünlü, Appl. Phys. Lett. **78**, 4071 (2001).
[26]I. Ichimura, S. Hayashi, and G. S. Kino, Appl. Opt. **36**, 4339 (1997).
[27]S. B. Ippolito, Ph.D. dissertation, Boston University, 2004.
[28]M. Born and E. Wolf, *Principles of Optics*, 7th ed. (Cambridge University Press, New York, 1999), pp. 465 and 159.
[29]S. M. Mansfield, W. R. Studenmund, G. S. Kino, and K. Osato, Opt. Lett. **18**, 305 (1993).
[30]C. J. R. Sheppard, J. Opt. Soc. Am. A **18**, 1579 (2001).
[31]E. Wolf, Proc. R. Soc. London, Ser. A **253**, 349 (1959).
[32]B. Richards and E. Wolf, Proc. R. Soc. London, Ser. A **253**, 358 (1959).
[33]A. J. d. Dekker and A. v. d. Bos, J. Opt. Soc. Am. A **14**, 547 (1997).
[34]P. Török, P. Varga, Z. Laczik, and G. R. Booker, J. Opt. Soc. Am. A **12**, 325 (1995).
[35]P. Török, P. Varga, and G. R. Booker, J. Opt. Soc. Am. A **12**, 2136 (1995).
[36]P. Török, P. Varga, A. Konkol, and G. R. Booker, J. Opt. Soc. Am. A **13**, 2232 (1996).
[37]T. D. Milster, J. S. Jo, and K. Hirota, Appl. Opt. **38**, 5046 (1999).
[38]J. S. Jo, T. D. Milster, and J. K. Erwin, Opt. Eng. (Bellingham) **41**, 1866 (2002).
[39]S. B. Ippolito, S. A. Thorne, M. G. Eraslan, B. B. Goldberg, M. S. Ünlü, and Y. Leblebici, Appl. Phys. Lett. **84**, 4529 (2004).
[40]J. C. Tsang and J. A. Kash, Appl. Phys. Lett. **70**, 889 (1997).
[41]J. C. Tsang, J. A. Kash, and D. P. Vallett, IBM J. Res. Dev. **44**, 583 (2000).
[42]S. Somani, S. Kasapi, K. Wilsher, W. Lo, R. Sobolewski, and G. Gol'tsman, J. Vac. Sci. Technol. B **19**, 2766 (2001).
[43]B. B. Goldberg, S. B. Ippolito, L. Novotny, Z. Liu, and M. S. Ünlü, IEEE J. Sel. Top. Quantum Electron. **8**, 1051 (2002).
[44]K. Ikushima, H. Sakuma, and S. Komiyama, Rev. Sci. Instrum. **74**, 4209 (2003).